Exp Fluids (2012) 53:1867–1877
DOI 10.1007/s00348-012-1403-4

RESEARCH ARTICLE

Dean-coupled inertial migration and transient focusing of particles in a curved microscale pipe flow

Kyung Won Seo · Yong Seok Choi · Sang Joon Lee

Received: 21 May 2012 / Revised: 6 October 2012 / Accepted: 7 October 2012 / Published online: 20 October 2012

Abstract The Dean-coupled inertial migration of neutrally buoyant spherical particles that are suspended in a curved microscale pipe flow was experimentally investigated in the range of $6.4 \leq \mathrm{Re} \leq 129$ and $1.69 \leq De \leq 34.1$. The three-dimensional positions of the particles were measured by using digital holographic microscopy. The diameter of the microtube was 350 μm, and the ratios of the tube diameter (D) to the particle diameter (d) were $D/d = 12$, 23, 35, and 50. Over a critical value of the *Focusing number* (F_C), the particles were initially tubular-pinched at the entrance of the curved region. The detailed structures of the Segré–Silberberg annulus as well as its deformation attributed to secondary flow were analyzed. Diverse agglomeration patterns of particles corresponding to the various flow conditions were observed. The optimal conditions that induced the particles to focus at a certain lateral position were determined.

1 Introduction

The focusing and enrichment processes for rarefied samples are important for increasing diagnostic sensitivity in numerous biological and chemical research fields. Several microfluidic devices have been developed to increase diagnostic sensitivity. However, the use of conventional methods, such as membrane filtration, gave rise to clogging problems and high maintenance costs. Several membraneless techniques that operate in continuous-flow modes and are free from the aforementioned problems have recently been developed (Bhagat et al. 2008; Di Carlo 2009; Jaggi et al. 2007; Kim and Yoo 2012; Wickramasinghe et al. 2001; Yang et al. 2006). These devices usually focus the particles into a tight stream by using hydrodynamic lateral forces that induce inertial migration. A particle that is subjected to shear flow migrates across the streamline because of inertia. Segre and Silberberg (1961) observed that a spherical particle in a pipe flow moves outward from the center and inward from the wall to a specific equilibrium position. Kim and Yoo (2009a, b) demonstrated the same phenomena by using charged particles and an electric field. Choi and Lee (2010) investigated the inertial migration of neutrally buoyant spherical particles, which were suspended in a microscale pipe flow at a Reynolds number range of $1.6 \leq Re \leq 77.4$ by using a digital holography technique. Particles in straight rectangular microchannels are focused at two or four symmetric equilibrium positions depending on the cross-sectional shape of the channel (Chun and Ladd 2006).

Kim and Yoo (2008) experimentally investigated the inertial migration of particles inside a square microchannel in the range of $0.06 \leq Re \leq 58.65$. Di Carlo et al. (2009) conducted experimental and numerical studies to account for the finite size of the suspended particles in a square channel. The three-dimensional (3D) positions of neutrally buoyant spherical particles inside a square microchannel were measured by using the digital holographic microscopy technique (Choi et al. 2011). In a theoretical study, Schonberg and Hinch (1989) calculated the inertial migration of a small sphere in a two-dimensional (2D) Poiseuille flow by using the matched asymptotic expansion

K. W. Seo · Y. S. Choi · S. J. Lee (✉)
Department of Mechanical Engineering,
Center for Biofluid and Biomimic Research,
Pohang University of Science and Technology,
Pohang 790-784, Korea
e-mail: sjlee@postech.ac.kr

K. W. Seo
e-mail: kwseo@postech.ac.kr

method. They found that the equilibrium position moves toward the wall as *Re* increases. Matas et al. (2004, 2009) investigated the inertial migration of particles at high *Re* ranges for a planar channel flow and a pipe flow in experimental and theoretical studies. Shao et al. (2008) investigated the inertial migration of spheres in a pipe flow in the range of $Re \leq 2{,}200$. They observed the inner equilibrium positions as *Re* exceeded a critical value. Chun and Ladd (2006) numerically simulated the inertial migration of particles inside a square duct in the range of $100 \leq Re \leq 1{,}000$.

The secondary Dean flow can be combined with the effect of inertial migration to reduce the number of equilibrium positions further. For example, curved or spiral microchannels have been demonstrated to create a single focused particle stream by inducing the interaction between the inertial lift and the Dean drag. Ookawara et al. (2006) numerically examined the development of particle concentration profiles over cross-sectional planes through a series of angular positions in a curved microchannel, which is the functional part of a microseparator. Studies by Bhagat et al. (2008) and Kuntaegowdanahalli et al. (2009) suggest an inertial microfluidic device that achieves continuous particle separation by using the principle of Dean-coupled inertial migration in spiral microchannels. However, in practice, curved or spiral microchannels have high costs because of their complex fabrication processes as well as the limited accessibility to expensive facilities. In addition, little is known about the Dean-coupled inertial migration of a particle. Thus, instead of using microchannels, we employed a flexible microtube, which is relatively inexpensive, for the basic study on the particle behavior and the purpose of simple sample focusing and enrichment.

The secondary Dean flows in a curved tube originate from the centrifugal hydrodynamic pressure imbalance in the main flow, which can be weighed by using the Dean number (*De*). The pressure imbalance generates fluid inertia that is directed toward the outward walls. The flow inertia is larger in the central region than in the near-wall regions because of flow velocity. The symmetric tube geometry induced the dual recirculation of the flow at the top and bottom halves of the tube cross-section to satisfy continuity, as shown in Fig. 1a. *De*, which describes the magnitude of the secondary flow, is defined as follows: $De = Re\sqrt{\delta}$, where δ is the ratio of the tube radius ($D/2$) to the radius of curvature (R_c), that is, $\delta = D/(2R_c)$ (Berger et al. 1983; Dean 1928; Kim and Lee 2009). The characteristic secondary flow velocity can then be scaled as $U_D \sim (De)^2(v/D)$, where v is the kinematic viscosity (Dean 1928). The Dean vortex flow in a curved pipe flow as well as its effect on the mass transfer through the liquid–liquid interface of two fluids is well studied numerically (Gelfgat et al. 2003).

The particles in the curved microtube exhibited both the inertial lift force (F_L) from the main streamwise flow and the Dean drag force (F_D) from the secondary flow. The particles tended to be positioned in the force-free region, where F_L and F_D are balanced. The technique of matched asymptotic expansions proved to be one of the most useful methods in determining dominant lateral forces on particles: $F_D = f_L \rho U_m^2 d^4/D^2$, where f_L is a non-dimensional lift coefficient, U_m is the streamwise mean flow velocity, and d is the particle diameter (Asmolov 1999; Matas et al. 2004; Schonberg and Hinch 1989). F_D can be estimated by using the Stokes drag given by $F_D = 3\pi\rho v d U_D = k\rho d U_m^2 D^2/R$, where k is a constant (Berger et al. 1983). The inertial equilibrium positions can be modified to a specific position where F_L and F_D are balanced, that is, $F_L \approx F_D$. However, given that f_L and the secondary flow velocity U_D strongly depend on the flow condition, the particle and channel

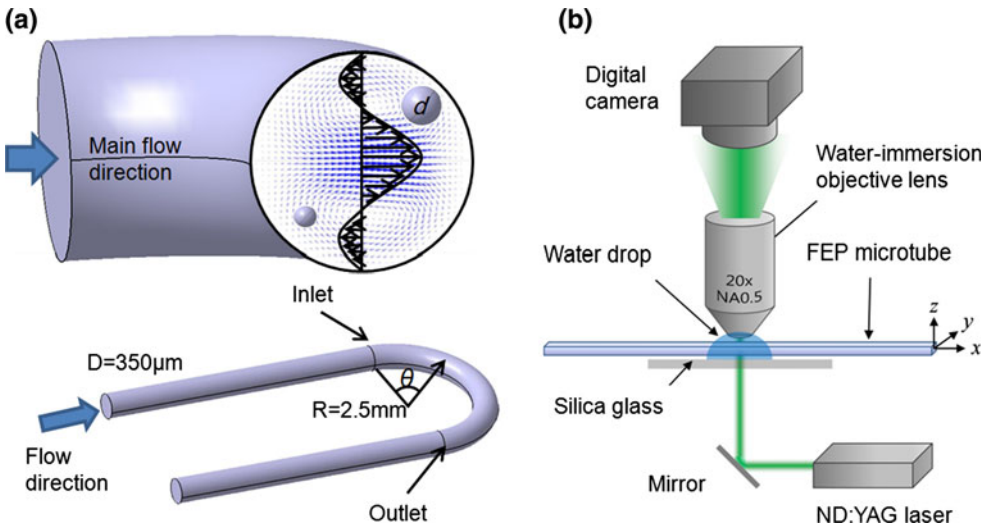

Fig. 1 **a** Configuration of the curved microtube with an inner diameter of 350 μm. The positional information of particles was measured at θ of 0°, 90°, and 180°. The Dean flow in a curved channel has two counter-rotating vortices that are perpendicular to the direction of the main flow. Suspended particles are subjected to Dean drag and inertial lift forces. The focusing positions of particles in curved channels are determined through the superposition of these two forces. **b** Schematic diagram of the experimental setup for digital holography

Table 1 Summary of experimental conditions

d (μm)	7	D/d		50
	10			35
	15			23
	30			12
Flow rate (μl/min)	Re	De (R_C = 2.5 mm, δ = 0.07)	De (R_C = 5 mm, δ = 0.035)	De (R_C = 7.5 mm, δ = 0.023)
100	6.4	1.69		
500	32.3	8.55	6.04	4.93
1,000	64.7	17.1	12.1	9.88
1,500	97	25.7	18.1	14.8
2,000	129	34.1	24.1	19.7

dimensions, and on the spatial position of the particle, the conditions required for the exact force balance are difficult to define clearly.

Although a number of experimental techniques have been employed in previous studies, most of these techniques are based on the point-wise scanning of the measurement area or on the 2D imaging of the mid-plane of a channel or pipe. An accurate measurement of particle motion in a circular pipe is especially difficult to achieve because of the curved surface of the pipe. Chun and Ladd (2006) have recently mentioned that the inertial migration of particles in a narrow channel is a fully 3D phenomenon. Therefore, a 3D measurement technique is ultimately required to measure the complex flow phenomena directly. In our previous study (Choi and Lee 2010), the lateral migration and tubular pinch effect of particles in a straight microtube were investigated at a certain Reynolds number (Re). In the present study, we obtained the 3D measurement of spherical particles transported through a curved microscale pipe flow by utilizing a digital holography technique for the basic study of particle motions as well as for simple particle focusing. We focused on Dean-coupled inertial migration and on the transient agglomeration of particles at the curved section of the tube. In addition, we experimentally investigated the effects of Re and De on the said phenomena.

2 Experimental conditions

The microtube in this study had a diameter D of 350 μm and was made of fluorinated ethylene propylene (FEP), which has a similar refractive index as that of water. The optical distortion attributed to refraction was prevented by immersing the tube in a water bath. The tube was bent at an angle of 180°, 30 cm downstream from the entrance. The 30 cm length ensured the fully developed state of radial migration under the experimental conditions. The radii of curvature (R_C) at the bending region were 2.5, 5.0, and 7.5 mm, and the corresponding ratios of the tube to the radius of curvature δ were 0.07, 0.035, and 0.023, respectively. Polystyrene microspheres with mean diameters d of 7, 15, and 30 μm were used as test particles. The particles were suspended in purified water with concentrations below 0.5 % in the volume fraction to disregard the particle–particle interactions. The density of water was then by using dissolved sodium chloride to achieve neutral particle buoyancy (ρ = 1.05 g/cm^3). Flow rates were adjusted by using a syringe pump, such that the value of Re was in the range of 6.4–129, and the corresponding value of De was in the range of 1.69–34.1. The experimental conditions are summarized in Table 1.

3 Digital holography

3.1 Digital holographic microscopy

In this study, the particle positions in the cross-sectional plane of a microtube are measured by using digital inline holographic microscopy (DIHM) (Choi and Lee 2010; Choi et al. 2011; Sheng et al. 2006). The DIHM method measures the 3D positional information of particles. Figure 1b shows a schematic diagram of the DIHM setup that comprises a continuous Nd:YAG laser (CrystaLaser, USA), a water-immersion objective lens (20×, NA = 0.50, Nikon, Japan), and a digital high-speed camera (Ultima-APX, Photron, Japan).

3.2 Numerical reconstruction of hologram

Prior to hologram reconstruction, the time-averaged background image is subtracted from the original raw holograms to eliminate the noises caused by optical components and misalignment. The background-subtracted hologram image is then numerically reconstructed to analyze the 3D positional information of the particles by employing the following Fresnel–Kirchhoff diffraction formula, which consists of the convolution between the hologram function $h(x, y)$ and the diffraction kernel $g(x, y)$ at each reconstruction plane:

$$\Gamma(\xi,\eta)=\frac{i}{\lambda}\int_{-\infty}^{\infty}\int_{-\infty}^{\infty}E_R(x,y)h(x,y)\frac{\exp\left(-i\frac{2\pi}{\lambda}\rho\right)}{\rho}\mathrm{d}x\mathrm{d}y \quad (1)$$

$$\rho=\sqrt{d^2+(\xi-x)^2+(\eta-y)^2}. \quad (2)$$

where ρ is the distance between a point in the hologram plane and a point in the reconstruction plane. The coordinate system of the numerical reconstruction is described in Fig. 2. Eq. 1 calculates the complex amplitude of the reconstructed wave field at a distance d from the hologram plane. To reconstruct the volume information of the object field, reconstruction should be performed through the whole volume with varying the reconstruction distance d.The Fresnel–Kirchhoff integral of Eq. 1 can be interpreted as a convolution of the hologram function $h(x, y)$ and of diffraction kernel $g(x, y)$:

$$\Gamma(\xi,\eta)=\{h(x,y)\otimes g(x,y)\}(\xi,\eta) \quad (3)$$

$$g(x,y)=\frac{i}{\lambda}\frac{\exp\left(-i\frac{2\pi}{\lambda}\sqrt{d^2+x^2+y^2}\right)}{\sqrt{d^2+x^2+y^2}}. \quad (4)$$

From the convolution theorem, the integral can be efficiently calculated by using the 2D fast Fourier transforms (FFTs) as follows:

$$\Gamma(\xi,\eta)=\Im^{-1}[\Im\{h(x,y)\}\Im\{g(x,y)\}] \quad (5)$$

where $\Im$ and $\Im^{-1}$ denote the FFT and inverse-FFT, respectively. The intensity field of the reconstructed images can be obtained by taking the absolute $|\Gamma(\xi,\eta)|$.

3.3 Determination of 3D particle position

After numerical reconstruction, the 3D positional information of the particles is determined. To identify the in-plane (x, y) positions of each particle, the center position of the particles that have higher intensity values than the background is investigated by using a local-peak-searching algorithm.

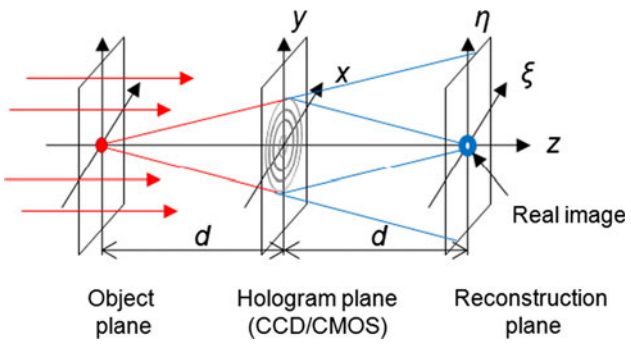

Fig. 2 Coordinate systems for the numerical reconstruction

After identifying the in-plane position of each particle, a rectangular section that encloses each particle is generated through particle segmentation. The size of each segment is determined to hold the neighboring pixels that exceed 80 % of the particle center intensity in the projection image. Each reconstructed particle image is then cropped along the rectangular section, and the corresponding focus value of each section is calculated by adopting an auto-focus function (Choi and Lee 2009). This process generates a list of focus values for each particle throughout the depth direction. Thus, the z-position of the particle can be determined as the peak position of each focus value profile. We used LAP as a focus function, which accounts for the variation in the intensity gradient defined as follows:

$$\mathrm{LAP}(z)=\sum_{x,y}\{\nabla^2 I(x,y;z)\}^2, \quad (6)$$

where $I(x, y, z)$ is the discrete intensity distribution of the segmented reconstruction image. A typical example of the focus value profiles that are obtained from reconstructed particle images is shown in Fig. 3.

4 Inertial migration in straight pipe flow

The inertial migration of the suspended particles at the entrance of the curved section ($\theta = 0°$) is initially investigated by adjusting the particle size and the value of *Re*.

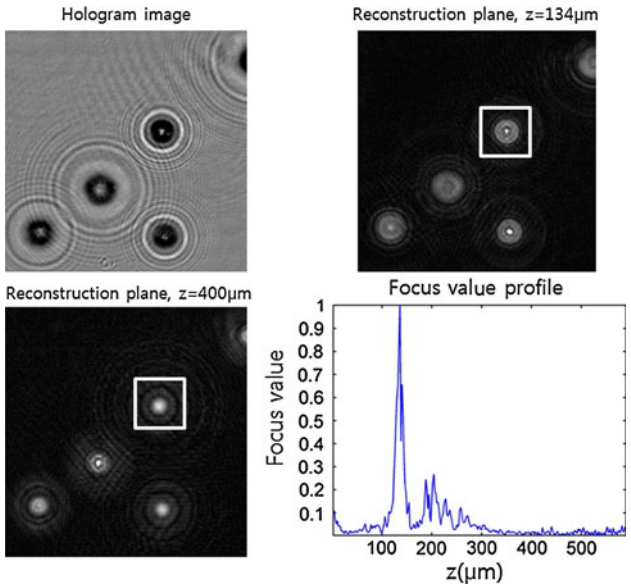

Fig. 3 Typical hologram image of 15 μm particles and the corresponding reconstructed images at different depthwise positions. Each particle is optimally focused at a certain z-position, where the corresponding focus value becomes the maximum. The particle surrounded by a *square box* is located 134 μm away from the focal plane, which corresponds with the result obtained from the focus value profile

Figure 4a shows the spatial distribution of the 15-μm particles ($D/d = 23$) at $\theta = 0°$. The particles accumulate around the central region of the tube at approximately $r/R < 0.6$ at the lowest Re of 6.4 because the hydrodynamic particle–wall interaction pushes the particles away from the wall. On the other hand, the particles in the central region migrate toward the wall when the value of Re increases because of the increased shear gradient force. The so-called tubular pinch effect consequently becomes distinct. Figure 5a shows the variations in the radial equilibrium position (r_{eq}), in which the particles are pinched, as a function of the Re and of the particle size ratio D/d. Under the present experimental conditions, r_{eq}/R varies from 0.55 to 0.73, where R is the radius of the tube ($R = D/2$). The r_{eq}/R value increases with increasing Re because of the increase in the outward F_L. The outward lift force is proportional to U_m^2, whereas the wall repulsion is proportional to U_m. With fixed Re, the r_{eq}/R decreases with increasing particle size because of the decrease in the gap between the particle and the tube wall, which significantly increases the hydrodynamic wall-repulsion force arising at the gap.

The specific condition under which the "tubular pinch effect" is fully developed by the inertial lift force is evaluated at the entrance of the curved region ($\theta = 0°$). In our previous study (Choi et al. 2011), we suggested a dimensionless parameter called "Focusing number" (F_c) that determines the flow condition for inertial focusing by balancing the inertial lift and the Stokes drag as follows: $f_L \rho U_m^2 d^4/D^2 = 3\pi U_{Dean} d$. In addition, Di Carlo et al. (2009) reported that the product of the inertial lift coefficient f_L and of the particle size ratio d/D can be fitted into a single curve as $f_L \times (d/D) = C_L$, in which C_L varies in the range of 0–0.04. By simply relating these two expressions, a ratio between the streamwise and lateral velocity components of a migrating particle can be deduced and the resultant traveling distances of the particle can be estimated directly as follows:

$$\frac{L_x}{L_l} \approx \frac{U_m}{U_l} = \frac{3\pi}{C_L Re_C (d/D)^2} \tag{7}$$

Given that the particle equilibrium position exists around 0.6–0.7 times half width of a channel, the

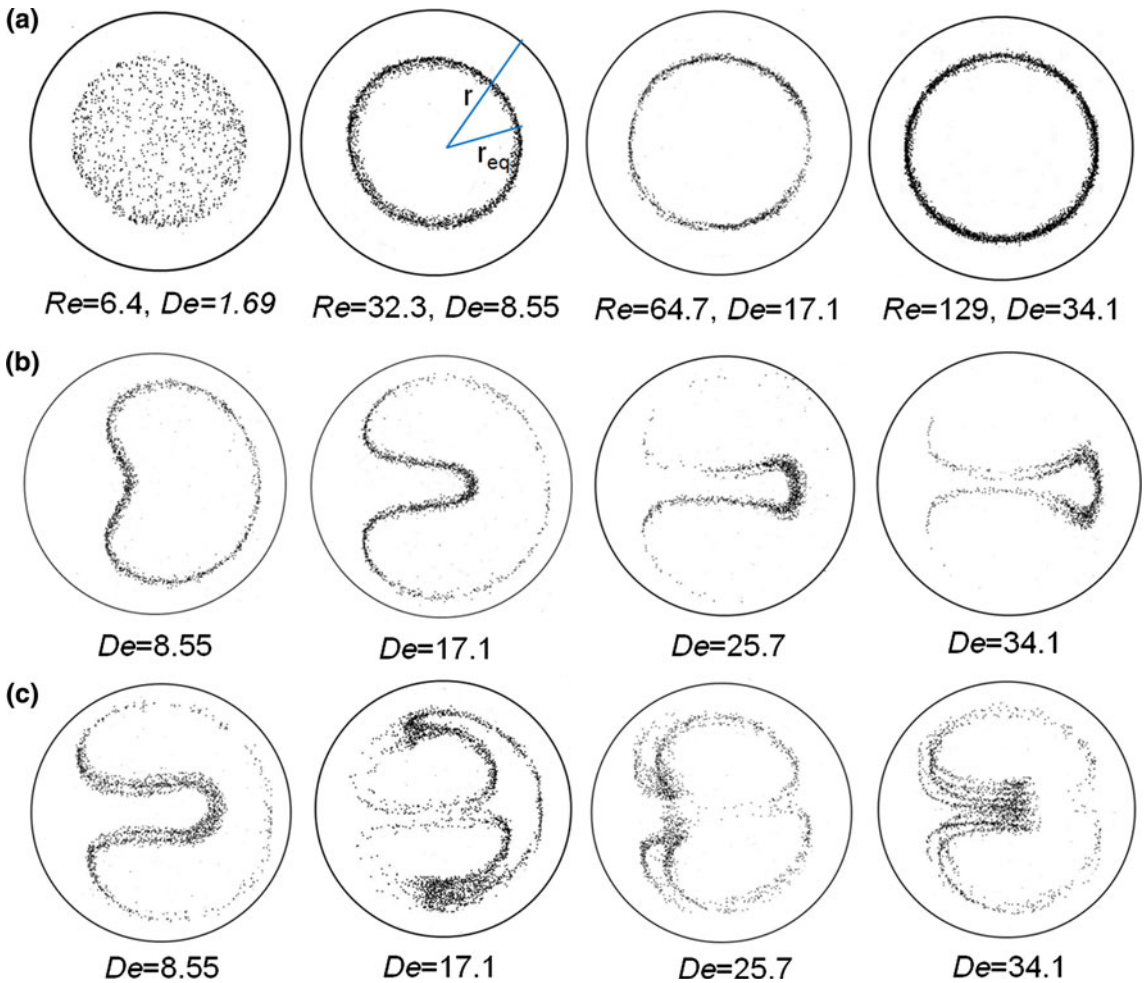

Fig. 4 Cross-sectional views of particle distributions ($D/d = 23$) flowing in a curved pipe ($\delta = 0.07$) at **a** $\theta = 0°$, **b** $\theta = 90°$, and **c** $\theta = 180°$

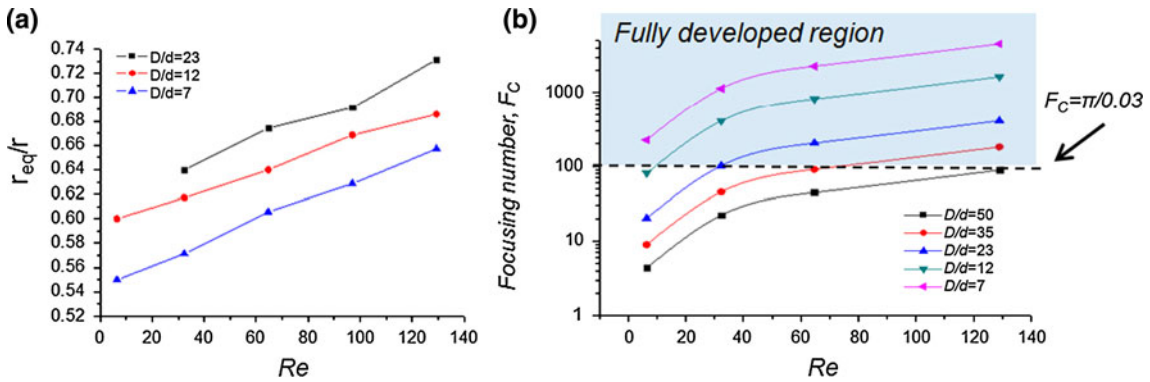

Fig. 5 **a** Variations in equilibrium positions (r_{eq}) according to the value of *Re*. **b** Variations in F_C with respect to the value of *Re* and of the particle distribution (*D*/*d*) at the entrance of the curved channel ($\theta = 0$). The inertial migration effect was fully developed when F_C was over 100

appropriate lateral migration distance L_l should be approximately 3*D*. Furthermore, the required L_E needs to be designed longer than the streamwise sweeping distance L_x. Thus, a dimensionless parameter F_C, which determines the inertial focusing flow condition, can be obtained by substituting these values into Eq. (6) as follows:

$$F_C \equiv Re_C \left(\frac{d}{D}\right)^2 \frac{L_E}{D} > \frac{\pi}{C_L}, \tag{8}$$

where Re_c is the channel Reynolds number at maximum flow velocity, L_E is the entrance length. The particles in a square channel are obviously fully focused on the lateral direction when F_c exceeds a certain critical value of $\pi/0.02$. Moreover, the cross-lateral focusing of particles on the four equilibrium positions of each surface of a square channel occurs when F_C exceeds a higher value of $\pi/0.01$ (Choi et al. 2011). Several F_C values are obtained from various *Re*, which is in the range of 6.4–129, and from various particle size ratios as shown in Fig. 5b. From the experimental observations, we verify that the tubular pinch effect is fully developed in a straight pipe flow over 100 of F_c, where C_L corresponds to 0.03.

5 Inertial migration combined with secondary flow effects

Experimentally, we tested a wide range of flow rates, $1.67 < De < 34$, by using a U-shaped, single-turned microscale pipe flow, where we systematically varied the radius of curvature (R_C) and particle size (*d*). The flow information and velocity field of secondary flow were investigated before studying the interaction between particles and flow. Figure 6 shows a typical velocity field of the secondary flow as well as the velocities of the main and secondary flows. Two large counter-rotating vortices that are perpendicular to the main flow are clearly observed. The fast-moving fluid along the horizontal midline of the

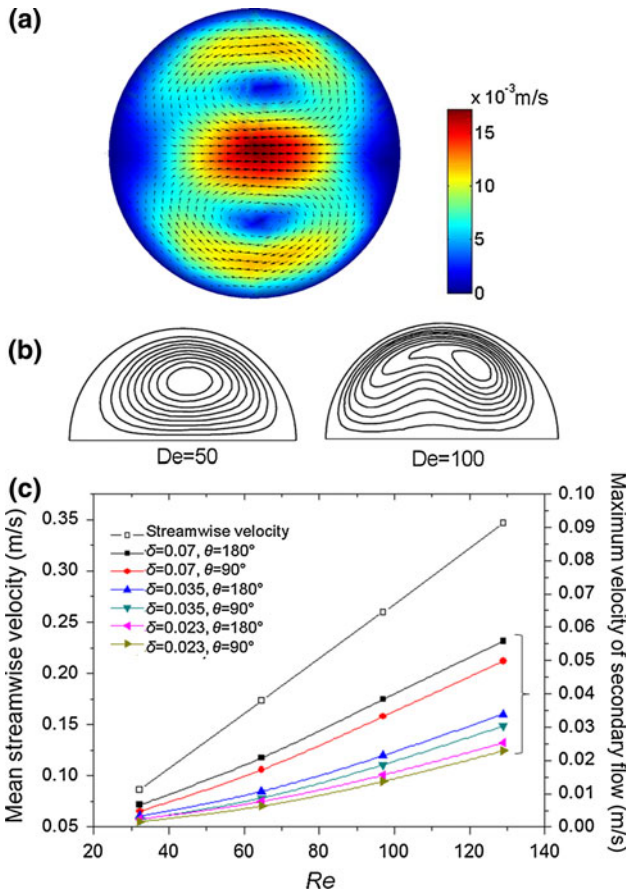

Fig. 6 Numerical analysis was conducted to investigate the secondary flow in a curved pipe by using the same numerical model with experiments. We conducted 3D, finite-element simulations that solve the steady-state Navier–Stokes equations in software (COMSOL Multiphysics). **a** Typical velocity field of secondary flow. The Dean number is 17.1, which corresponds to a Reynolds number of 64.7 in the tube ($\theta = 90°$) with a diameter (*D*) of 350 μm and a radius of curvature (R_C) of 2.5 mm. **b** Instantaneous iso-velocity contours of the secondary flow at $\theta = 90°$, where the tube diameter (*D*) is 300 μm (Kim and Lee 2009). **c** Variation of the mean streamwise velocity and the maximum velocity of secondary flow in a curved circular tube ($D = 350$ μm) as a function of the Reynolds number, the ratio of tube diameter to radius of curvature (δ) and θ

tube cross-section is directed outwards, whereas the slow-moving fluid along the top and bottom walls of the tube is directed inwards, as shown in Fig. 6a.

In our previous study (Kim and Lee 2009), Dean flow in a curved microtube ($D = 300$ μm) was measured using digital holographic particle tracking velocimetry (DHPTV) technique in the range of $5 \leq De \leq 100$. For the case of $De = 50$, the center of the large-scale counter-rotating vortex is located close to the center of the half-region of the microtube, as shown in Fig. 6b. As the Dean number increases, the center of the large-scale vortex moves toward the outer bend and the iso-velocity contours of the secondary flow in the central region of the microtube are bent upward. With increasing *De*, additional small-scale vortex structures are developed. Gelfgat et al. (2003) found a similar structure of the transverse flow (Dean vortices) numerically by using finite volume method. In the present study, the interaction between the secondary flow and particles was investigated in the range of $1 < De < 34$, corresponding to the case of low *De* in the previous study. Therefore, the flow conditions of the present study can be regarded as a steady-state, two large-scale counter-rotating vortices called as classical Dean flow.

The drag force exerted on a particle in the orthogonal direction relative to the mainstream can be obtained by assuming the Stokes drag as follows: $F_D = 3\pi U_{Dean} d$. Therefore, the rate of particle transportation across the main flow is directly proportional to the local velocity of the secondary flow.

The secondary flow deforms the particle trajectories when the tubular-pinched particles pass through the curved section of the tube. The deformation of the circular particle annulus depends on the measurement location (θ) and on the value of *De*. The particle annuli, which are initially circular, were observed to change, and the unique agglomeration patterns of the particles appeared. Figure 4b, c shows the cross-sectional position of the particles at two cross-sections with θ of 90° and 180°, respectively, and with varying values of *De*. Initially, the particles ($d = 15$ μm, $D/d = 23$) located near the inner bend (left side) start to migrate toward the outer bend (right side) along the horizontal midline of the tube cross-section at $De = 8.55$, as shown in Fig. 4b. The particles that are positioned near the outer bend are swept along the top and bottom walls of the tube, and outward migration along the midline is further developed as *De* increases (Fig. 4). The cross-lateral migration of particles across the main flow is further developed at $\theta = 180°$ compared with those at $\theta = 90°$, as shown in Fig. 4c. The particle migration exhibits diverse distribution patterns according to *De* and θ.

The local particle distribution was evaluated by using the probability density function (PDF). Figure 7 represents the PDF distributions, where the locally concentrated regions are prominently colored red. The particles tend to agglomerate at a narrow cross-sectional region near the outer bend when $\theta = 90°$ and when *De* is in the range of 25–34. The particles exhibit gradual migration with various agglomeration patterns as they are transported downstream of the curved region and as *De* increases. Although the local concentrations at $\theta = 180°$ are not extremely high, the particles focus around the inner bend or the center region when the value of *De* is properly controlled in the range of 17–34, as shown in Fig. 7b.

Under the critical value of F_C for the condition of the fully developed tubular pinch effect, the agglomeration

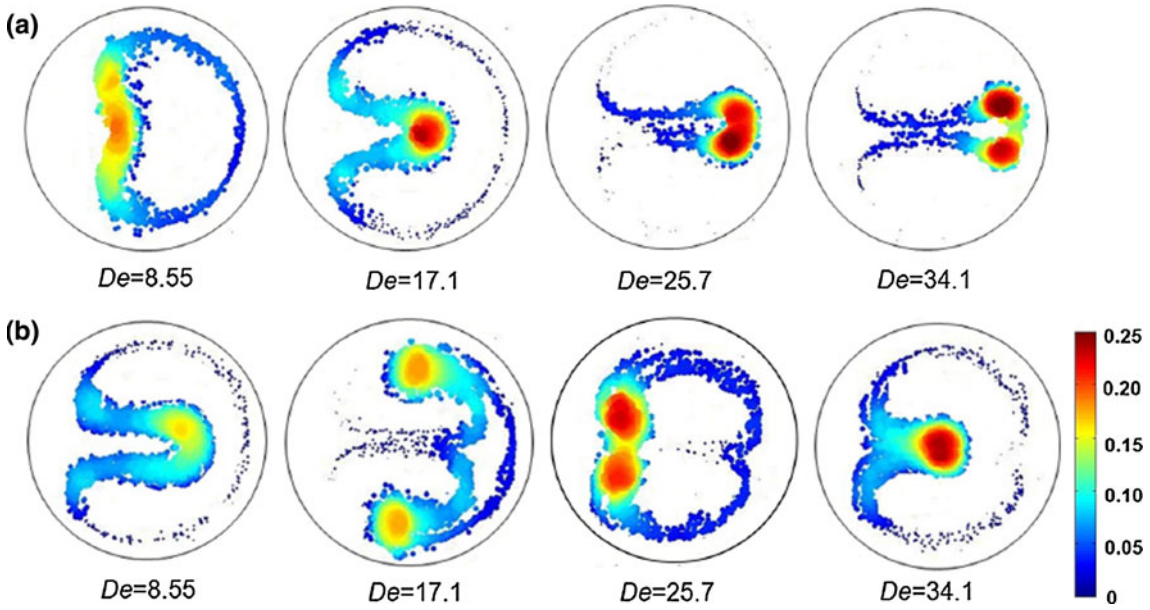

Fig. 7 Normalized particle distributions in a curved tube ($D/d = 23$, $\delta = 0.07$) at the cross-sections of **a** $\theta = 90°$ and **b** $\theta = 180°$

patterns do not appear in the curved region, and the particles are affected mainly by the Dean drag force compared with the inertial lift force ($F_D \gg F_L$). Such a phenomenon can be attributed to low *Re*, insufficient entry length, and small particle size compared with channel dimension; for instance, the inertial lift force exerted on a particle is insufficient because of small particle size and low *Re* ($d = 7$ μm, $F_C = 22$–88). Thus, the agglomeration patterns do not appear clearly, as shown in Fig. 9a. At a high *De* value, the inertial lift force can be disregarded versus the Dean drag force ($F_D \gg F_L$). Therefore, the mixing process attributed to secondary flow is dominant, and

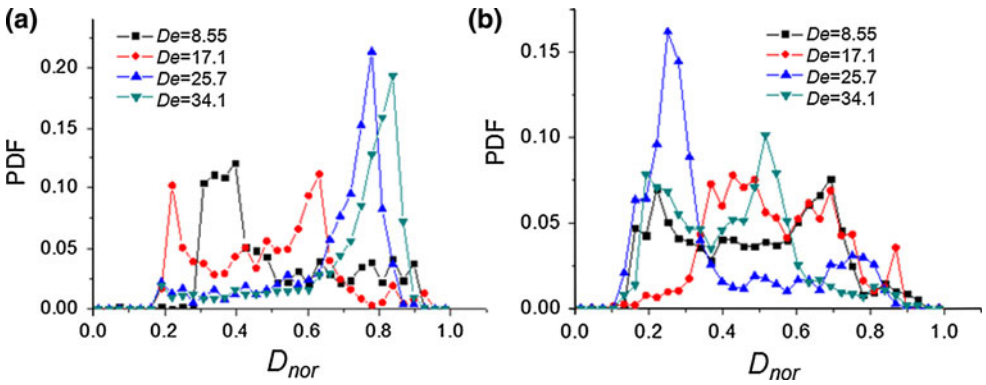

Fig. 8 Lateral PDF distributions of the particles across the microtube at **a** $\theta = 90°$ and **b** $\theta = 180°$

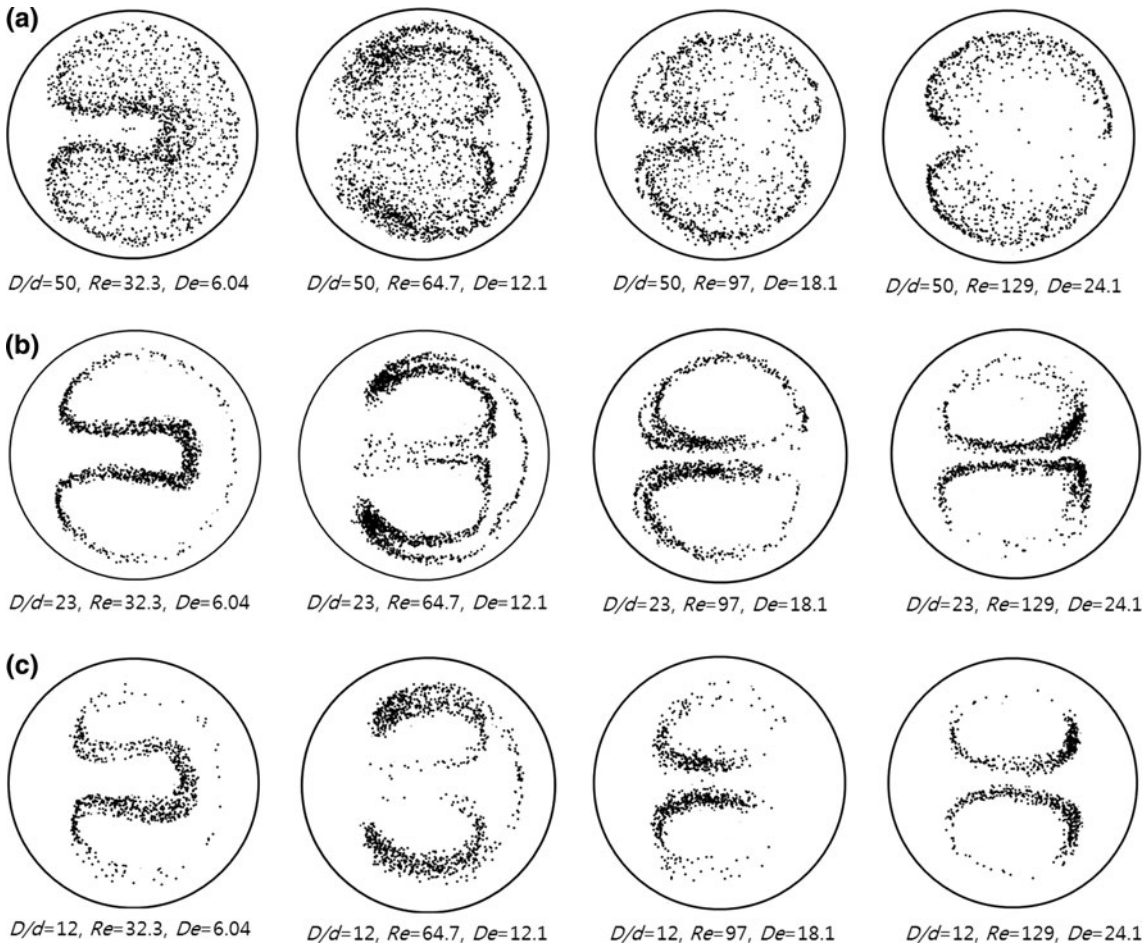

Fig. 9 Effects of particle size on the particle migration flowing in a curved circular microtube. Cross-sectional distributions of stationary particles **a** $D/d = 50$, **b** $D/d = 23$, **c** $D/d = 12$ in a curved tube at $\theta = 180°$, $\delta = 0.035$. In the case of (**a**) a small particle ($d = 7$ μm) and a low Reynolds number, particle migration is not fully developed because of insufficient inertial lift force. Despite the different ratios of particles and of the channel diameter, the migration pattern is similar under the same flow conditions

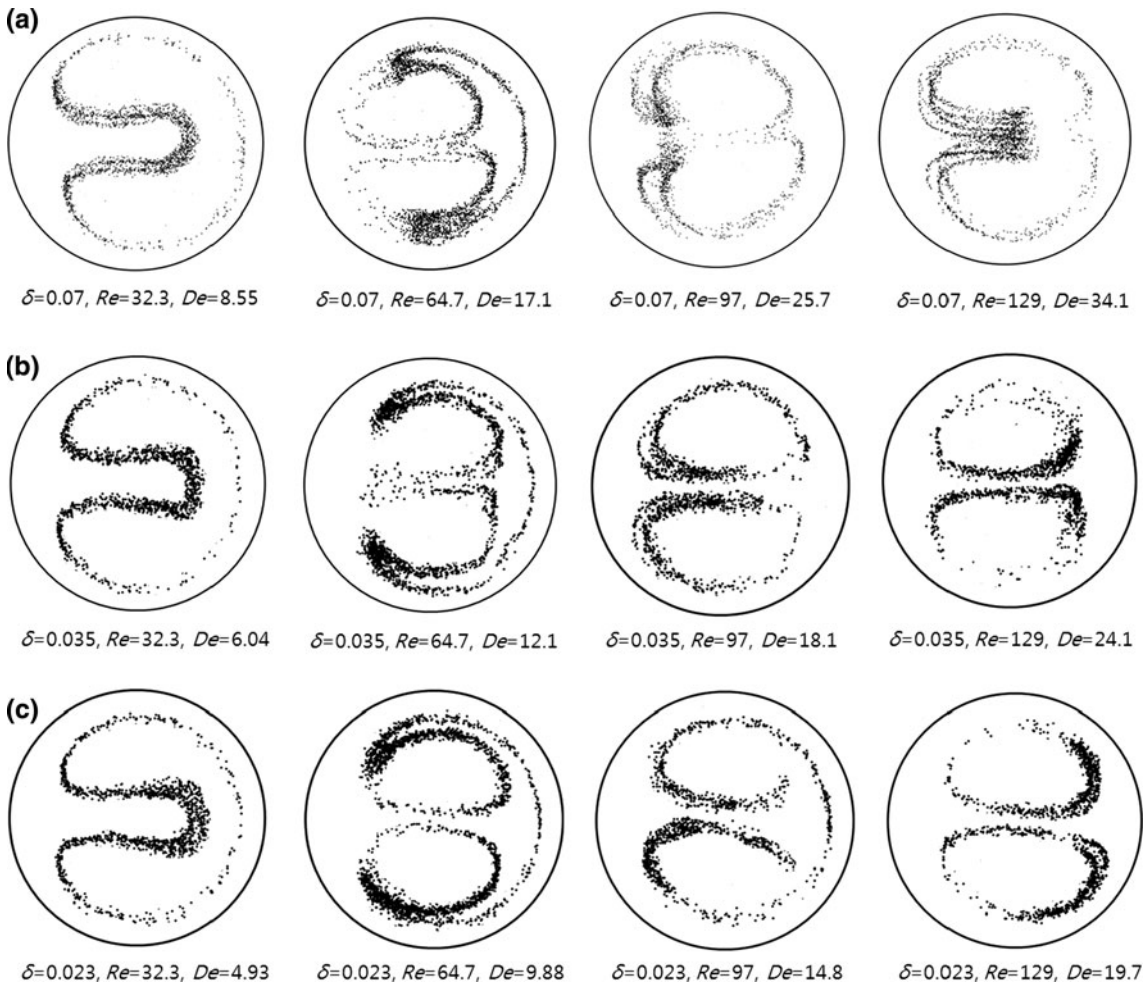

Fig. 10 Effects of the ratio of channel diameter to radius of curvature (δ) on the particles ($D/d = 23$) migrating in a curved circular tube. Cross-sectional distributions of stationary particles **a** $\delta = 0.07$, **b** $\delta = 0.035$, and **c** $\delta = 0.023$ in a curved tube at $\theta = 180°$

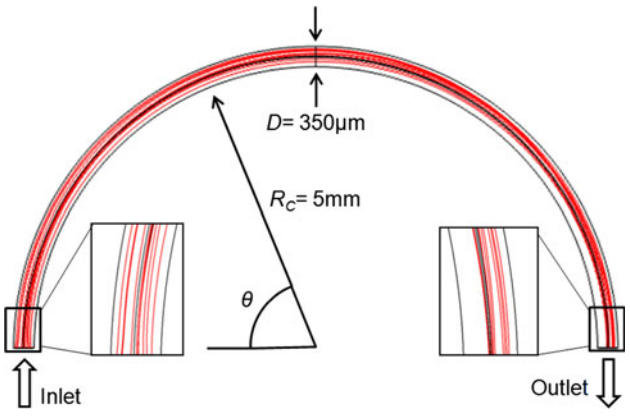

Fig. 11 Trajectories of particles ($d = 30$ μm) at $Re = 51.2$ and $De = 9.6$. Most particles pass through the half plane near the outer wall in the cross-section at the outlet of curved section

particle agglomeration is destroyed. These observations imply that transient particle focusing can occur at a moderate range of flow conditions ($F_D \approx F_L$).

Figure 8 shows the top view (general 2D observation) of the PDFs of the particles along the lateral axis of the tube with θ of 90° and 180°, respectively. D_{nor} represents the lateral position normalized by the tube diameter. The PDF distributions show the accumulation of particles at certain lateral positions. When $\theta = 90°$ and the value of De is in the range of 25–34, most particles accumulate in the region near the outer wall of the tube (D_{nor} of 0.7–0.8). In addition, the particles accumulate near the inner bend (D_{nor} of 0.25) when $\theta = 180°$ and De is 25.7.

The effects of particle size (d) and the radius of curvature (R_c) were investigated by using spherical particles with d of 7, 15, and 30 μm and curved tubes with R_c of 2.5, 5, and 7.5 mm, respectively. Figures 9 and 10 show the spatial distributions of particles for the aforementioned cases. As shown in Fig. 9a, in the case of small particles ($d = 7$ μm), the focusing patterns of the particles are not evident because the inertial lift force is insufficient to establish a fully developed particle annulus at the entrance of the curved section. On the other hand, in the case of a

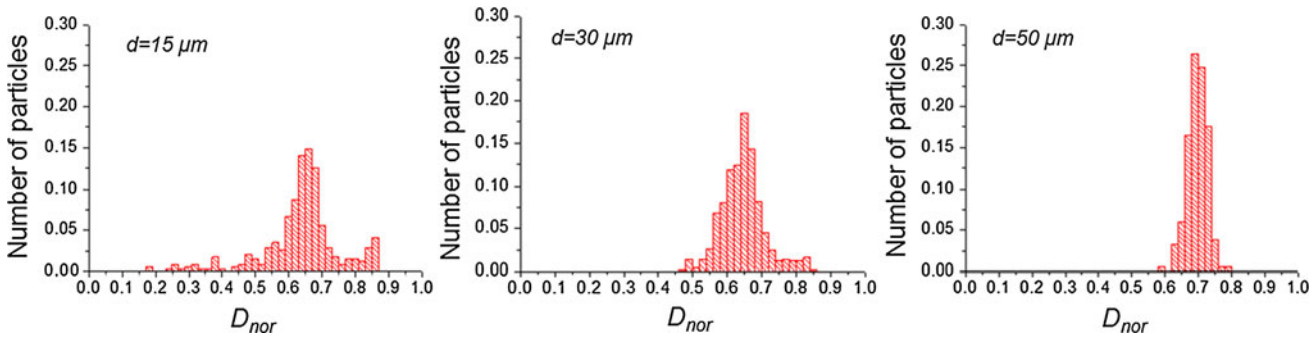

Fig. 12 Histograms illustrating the normalized number of particles across the tube outlet at $Re = 51.2$ and $De = 9.6$

sufficiently large particle size, similar agglomeration patterns of the particles are clearly observed under the same *Re* conditions (Fig. 9b, c) because the lift force exerted on a particle is proportional to the particle size. Interestingly, the similar focusing patterns of the particles are observed at the different radii of curvatures and ratios between a particle and tube diameter under modulate flow conditions.

We demonstrate the obtainment of a single particle stream by using a U-turned curved tube with an R_C of 5 mm ($\delta = 0.035$) and sphere particles with d of 15, 30, 50 μm at the tube outlet ($\theta = 180°$). The flow condition can be controlled to obtain similar cross-sectional particle distributions for $De = 25.7$–34.1 for a single particle stream near the outer wall of the tube outlet, as shown in Fig. 7a. Figure 11 represents the trajectories of particles ($d = 30$ μm) passing through the curved pipe flow at $Re = 51.2$, where the corresponding *De* value is 9.6. Most particles pass through the half plane near the outer wall in the cross-section at the outlet of the curved section. To get more detailed statistical information on the particle focusing at the tube outlet, the histogram of the normalized number of particle across the tube outlet was extracted, as shown in Fig. 12. The values 0 and 1 of D_{nor} represent the inner and outer walls, respectively. The lateral positions of particles over 1,000 are measured for each case. The three different sizes of particles are well focused at D_{nor} values from 0.6 to 0.8. Particularly, in the case of $d = 50$ μm, particles are focused at a narrow stream near the outer wall, where more than 80 % of particles are focused at $D_{nor} = 0.7 \pm 0.04$.

6 Conclusions

In this study, we experimentally investigated the Dean-coupled inertial migration and transient focusing of particles in curved microscale pipe flows by using a 3D imaging technique under varying flow conditions. The randomly suspended particles formed a circular annulus in the straight entrance section of the tube and were subsequently deformed by the secondary flow in the curved section. The particles were focused in a narrow cross-sectional position under a specific flow condition. The particle focusing position can be controlled and adjusted by properly tailoring the curve and flow conditions. We demonstrated particle focusing on a narrow stream at the exit of the curved pipe flow. This phenomenon can be used as a simple method for particle focusing to make sample diagnoses in microfluidic devices easier.

Acknowledgments This research was supported by the World Class University Program (R31-2008-000-10105-0) and the Creative Research Initiatives (Diagnosis of Biofluid Flow Phenomena and Biomimic Research) of the National Research Foundation of Korea, funded by the Ministry of Education, Science, and Technology.

References

Asmolov ES (1999) The inertial lift on a spherical particle in a plane Poiseuille flow at large channel Reynolds number. J Fluid Mech 381:63–87

Berger SA, Talbot L, Yao LS (1983) Flow in curved pipes. Annu Rev Fluid Mech 15:461–512

Bhagat AAS, Kuntaegowdanahalli SS, Papautsky I (2008) Continuous particle separation in spiral microchannels using dean flows and differential migration. Lab Chip 8:1906–1914. doi:10.1039/B807107a

Choi YS, Lee SJ (2009) Three-dimensional volumetric measurement of red blood cell motion using digital holographic microscopy. Appl Opt 48:2983–2990

Choi YS, Lee SJ (2010) Holographic analysis of three-dimensional inertial migration of spherical particles in micro-scale pipe flow. Microfluid Nanofluid 9:819–829. doi:10.1007/s10404-010-0601-8

Choi YS, Seo KW, Lee SJ (2011) Lateral and cross-lateral focusing of spherical particles in a square microchannel. Lab Chip 11:460–465. doi:10.1039/C0lc00212g

Chun B, Ladd AJC (2006) Inertial migration of neutrally buoyant particles in a square duct: an investigation of multiple equilibrium positions. Phys Fluids 18:031704. doi:10.1063/1.2176587

Dean WR (1928) Fluid motion in a curved channel. Proc R Soc Lond A 121:402–420

Di Carlo D (2009) Inertial microfluidics. Lab Chip 9:3038–3046. doi:10.1039/B912547g

Di Carlo D, Edd JF, Humphry KJ, Stone HA, Toner M (2009) Particle segregation and dynamics in confined flows. Phys Rev Lett 102:094503. doi:10.1103/Physrevlett.102.094503

Gelfgat AY, Yarin AL, Bar-Yoseph PZ (2003) Dean vortices-induced enhancement of mass transfer through an interface separating two immiscible liquids. Phys Fluids 15:330–347. doi:10.1063/1.1532732

Jaggi RD, Sandoz R, Effenhauser CS (2007) Microfluidic depletion of red blood cells from whole blood in high-aspect-ratio microchannels. Microfluid Nanofluid 3:47–53. doi:10.1007/s10404-006-0104-9

Kim S, Lee SJ (2009) Measurement of Dean flow in a curved microtube using micro digital holographic particle tracking velocimetry. Exp Fluids 46:255–264. doi:10.1007/s00348-008-0555-8

Kim YW, Yoo JY (2008) The lateral migration of neutrally-buoyant spheres transported through square microchannels. J Micromech Microeng 18:065015. doi:10.1088/0960-1317/18/6/065015

Kim YW, Yoo JY (2009a) Axisymmetric flow focusing of particles in a single microchannel. Lab Chip 9:1043–1045. doi:10.1039/B815286a

Kim YW, Yoo JY (2009b) Three-dimensional focusing of red blood cells in microchannel flows for bio-sensing applications. Biosens Bioelectron 24:3677–3682. doi:10.1016/j.bios.2009.05.037

Kim YW, Yoo JY (2012) Transport of solid particles in microfluidic channels. Opt Lasers Eng 50:87–98

Kuntaegowdanahalli SS, Bhagat AAS, Kumar G, Papautsky I (2009) Inertial microfluidics for continuous particle separation in spiral microchannels. Lab Chip 9:2973–2980. doi:10.1039/B908271a

Matas JP, Morris JF, Guazzelli E (2004) Inertial migration of rigid spherical particles in Poiseuille flow. J Fluid Mech 515:171–195. doi:10.1017/S0022112004000254

Matas JP, Morris JF, Guazzelli E (2009) Lateral force on a rigid sphere in large-inertia laminar pipe flow. J Fluid Mech 621:59–67. doi:10.1017/S0022112008004977

Ookawara S, Street D, Ogawa K (2006) Numerical study on development of particle concentration profiles in a curved microchannel. Chem Eng Sci 61:3714–3724. doi:10.1016/j.ces.2006.01.016

Schonberg JA, Hinch EJ (1989) Inertial migration of a sphere in Poiseuille flow. J Fluid Mech 203:517–524

Segre G, Silberberg A (1961) Radial particle displacements in Poiseuille flow of suspensions. Nature 189:209–210

Shao XM, Yu ZS, Sun B (2008) Inertial migration of spherical particles in circular Poiseuille flow at moderately high Reynolds numbers. Phys Fluids 20:103307. doi:10.1063/1.3005427

Sheng J, Malkiel E, Katz J (2006) Digital holographic microscope for measuring three-dimensional particle distributions and motions. Appl Opt 45:3893–3901

Wickramasinghe SR, Lin WC, Dandy DS (2001) Separation of different sized particles by inertial migration. Biotechnol Lett 23:1417–1422

Yang S, Undar A, Zahn JD (2006) A microfluidic device for continuous, real time blood plasma separation. Lab Chip 6:871–880. doi:10.1039/B516401j